Multistatic Radar Change Detection Using A Sparse Imaging Approach

Mike Brennan and Chris Kreucher
The Fusion Group
Integrity Applications Incorporated
900 Victors Way, Suite 220, Ann Arbor MI 48108
{mbrennan, ckreucher}@integrity-apps.com

***Abstract*—This paper describes a sparse imaging approach for estimating change images from a constellation of multistatic radar. In our setup, radar antennas are arranged around the perimeter of a surveillance region. This provides large angular diversity but a very small angular sampling. Conventional backprojection imaging techniques applied to this data produce sidelobes which severely limit the utility of the imagery. We describe an innovative change imaging method which enforces sparseness on the estimated image. The method is illustrated with collected multistatic radar data, showing that the sparseness model produces excellent images with very limited sampling of the aperture.**

I. INTRODUCTION

This paper describes a novel method of exploiting data from a constellation of Radio Frequency (RF) sensors to image a region. In contrast to Synthetic Aperture Radar (SAR) imaging [1] which has small angular diversity but a very finely filled in aperture, in our setup we have large angular diversity, but the aperture is very poorly filled in (see Figure 1). Since the aperture is so dramatically undersampled (relative to the Nyquist requirement), traditional imaging techniques like backprojection result in a very poor image.

Our approach is to form an image of the changes between a reference collection and a new collection. The change image setting ensures that the image will be sparse, and allows us to use a sparseness model to constrain the estimate. This physical model enables estimation with fewer measurements than conventional Nyquist criteria would demand. In practice, we find excellent imaging with very limited sampling of the aperture.

Other authors have developed related approaches. For example, [2][3][4] apply sparse signal recovery techniques discussed in the compressed sensing literature to SAR imaging to deal with missing data and perform super-resolution imaging. Other authors [5][6] have looked at employing multistatic radar for enhanced imaging. Our approach differs from these and other works in that we exploit an undersampled (but wide) aperture from a constellation of multistatic radar to perform change imaging.

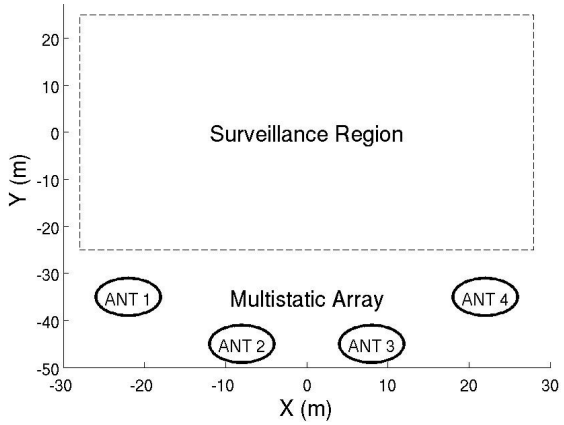

Figure 1. The Imaging Setting. 4 antennas give 12 bistatic pairs (6 are unique). This gives large angular diversity which is sparsely sampled.

The paper proceeds as follows. First, Section II describes the mathematics of our sparse change image algorithm and its implementation. Next, Section III shows field collects which employ four multistatic radar units, comparing the performance of the proposed sparse-model imaging algorithm with conventional backprojection imaging. Finally, Section IV concludes.

II. RANGE-DOMAIN SPARSE MODEL IMAGING

Our approach is to create an image of the changes over an *XY* region. This is done by collecting multistatic RF data both before and after a change event occurs and estimating the change in scene content from the change in bistatic range measurements. This section develops the notation and mathematics that describe the approach.

A. Notation

The surveillance region is discretized into a set of pixels. For the purpose of exposition, we assume here that the region is rectangular and evenly sampled, although these assumptions are not a requirement of the approach.

Formally, let the region be defined by $x \in \{x_{min}, x_{max}\}$, $y \in \{y_{min}, y_{max}\}$, and spacings δx and δy. Let N_x and N_y be the number of grid points in the X and Y directions, respectively. The surveillance region then has $N_x N_y$ pixels,

This work was supported by AFRL contract FA8650-10-C-1718.

each of which is contains an unknown change in Radar Cross Section (RCS) that we wish to estimate. Let $\underline{x}$ denote the $N_x N_y \times 1$ vector of unknowns, which will be organized x-coordinate major, i.e.,

$$\underline{x} \leftrightarrow \begin{bmatrix} x_{min}, y_{min} \\ x_{min}, y_{min} + \delta_y \\ \vdots \\ x_{min}, y_{max} \\ x_{min} + \delta_x, y_{min} \\ x_{min} + \delta_x, y_{min} + \delta_y \\ \vdots \\ x_{min} + \delta_x, y_{max} \\ \vdots \\ x_{max}, y_{max} \end{bmatrix}, \quad (1)$$

so the j^{th} element ($j = 1, \cdots, N_x N_y$) of $\underline{x}$, denoted $\underline{x}_j$, corresponds to a cell in the imaging region centered at

$$\begin{aligned} x_j &= x_{min} + \delta x \lfloor (j-1)/N_y \rfloor \\ y_j &= y_{min} + \delta y \, rem(j-1, N_y), \end{aligned} \quad (2)$$

where $\lfloor \cdot \rfloor$ is the floor function and $rem(a, b)$ is the remainder when a is divided by b. The index j will be used with the unknown $\underline{x}$ and always refer to a spatial coordinate.

Measurements are made by the multistatic constellation both before and after a change. Let T be the number of transmitters and R be the number of receivers. Through Fourier processing, the raw measurements from each transmit/receive pair correspond to complex values in N_r bistatic range bins (assumed to be the same for all transmitter/receiver pairs for notational convenience). The complex-valued difference between observations before and after the change event in range bin k between transmitter t_x and receiver r_x will be denoted $\Delta r_k^{t_x \to r_x}$. In practice, this value is computed by averaging over many calibrated pulses before and after the change event.

The $TRN_r \times 1$ vector $\underline{b}$ is then the collection of changes $\Delta r_k^{t_x \to r_x}$, arranged range-bin major and transmitter minor:

$$\underline{b} = \left[\Delta r_1^{1\to 1} \cdots \Delta r_{N_r}^{1\to 1} \cdots \Delta r_1^{1\to 2} \cdots \Delta r_1^{T\to R} \cdots \Delta r_{N_r}^{T\to R} \right]^T. \quad (3)$$

The i^{th} element of $\underline{b}$, denoted $\underline{b}_i$, defines the bistatic range bin β_i, transmitter $t_{x,i}$ and receiver $r_{x,i}$ as

$$\begin{aligned} \beta_i &= 1 + rem(i-1, N_r), \\ t_{x,i} &= 1 + \lfloor (i-1)/RN_r \rfloor, \quad \text{and} \\ r_{x,i} &= 1 + rem(\lfloor (i-1)/N_r \rfloor, R). \end{aligned} \quad (4)$$

The index i will be used exclusively $\underline{b}$ and always refer to a range bin, transmitter, receiver combination.

B. *Mapping from Esimatee x to Observation b*

This section develops the model of how changes in the surveillance region $\underline{x}$ are reflected in the measurements $\underline{b}$.

From the bistatic radar equation [9], the received power P_r is related to the transmitted power P_t though the wavelength λ, receiver and transmitter gains G_t and G_r and ranges to the transmitter and receiver r^{Tx} and r^{Rx} by

$$P_r = \frac{P_t G_t G_r \lambda^2}{(4\pi)^3 (r^{Tx})^2 (r^{Rx})^2}. \quad (5)$$

The phase depends on the total bistatic range [11] and wavelength as $(r^{Tx}+r^{Rx})/\lambda$. In our notation, surveillance region index j maps to a location (x_j, y_j) as defined in eq. (2), and measurement index i corresponds to transmitter $t_{x,i}$ and receiver $r_{x,i}$ as defined in (4). Denote the transmitter and receiver locations by $\left(x_{t_x,i}, y_{t_x,i}\right)$ and $\left(x_{r_x,i}, y_{r_x,i}\right)$. Then the range between surveillance region index j and the transmitter and receiver associated with i are

$$\begin{aligned} r_{ij}^{Tx} &= \sqrt{\left(x_j - x_{t_x,i}\right)^2 + \left(y_j - y_{t_y,i}\right)^2} \\ r_{ij}^{Rx} &= \sqrt{\left(x_j - x_{r_x,i}\right)^2 + \left(y_j - y_{r_y,i}\right)^2}, \end{aligned} \quad (6)$$

and the total bistatic range between surveillance region index j and a transmitter/receiver specified by i is

$$r_{ij} = r_{ij}^{Tx} + r_{ij}^{Rx}. \quad (7)$$

The bistatic range r_{ij} corresponds to bistatic range bin

$$\rho_{ij} = 1 + mod\left(\lfloor r_{ij}/\delta_r \rfloor, \rho_{amb}\right), \quad (8)$$

where δ_r is the range bin spacing given by the speed of transmission and radar bandwidth ($\delta_r = c/BW$) and ρ_{amb} is the maximum unambiguous range bin, given by the bandwidth and the step frequency size ($p_{amb} = BW/\Delta f$).

With this as background, we can now precisely define the forward model $\underline{\underline{A}}$, which is a $TRN_r \times N_x N_y$ matrix that maps changes at (x_j, y_j) locations to observed changes in bistatic range measurements $\Delta r_k^{t_x \to r_x}$. The model is

$$\underline{b} = \underline{\underline{A}}\underline{x}. \quad (9)$$

For a test cell j and transmitter/receiver defined by i, the elements $\underline{\underline{A}}_{ij}$ reflect the gain and phase due to the bistatic range from the pair to the test cell. It has non-zero elements only when a spatial location implied by j maps to the bistatic range bin defined by i in the transmitter/receiver pair defined by i, i.e., where $\rho_{ij} = \beta_i$.

Let r_i^0 denote the range to scene center for a transmit receive pair indicated by i. Then, from this analysis the elements of $\underline{\underline{A}}$ are

$$\underline{\underline{A}}_{ij} = \begin{cases} G_{ij} \frac{e^{-\sqrt{-1}4\pi f\left(r_{ij} - r_i^0\right)/c}}{r_{ij}^{Tx} r_{ij}^{Rx}} & \rho_{ij} = \beta_i \\ 0 & otherwise \end{cases}, \quad (10)$$

where G_{ij} captures antenna gains, transmit power and other constants. The values are set via a calibration collect. The matrix $\underline{\underline{A}}$ acts as a selection operator, choosing which ij are non-zero by determining how ground pixels correspond to range measurements.

In practice (x_j, y_j) does not correspond precisely to a range bin center, so its energy will spread to neighboring bins. This is approximated in our model by using

$$\underline{\underline{A}}_{ij} = \begin{cases} \alpha_{ij} G_{ij} \frac{e^{-\sqrt{-1}4\pi f\left(r_{ij}-r_i^0\right)/c}}{r_{ij}^{Tx} r_{ij}^{Rx}} & \left|\rho_{ij} - \beta_i\right| < M \\ 0 & otherwise \end{cases} \quad (11)$$

where M is a gate size and α_{ij} is a weight function.

C. Sparse Change Image Reconstruction

The previous sections have defined the estimatee (change image) $\underline{x}$, the measurements $\underline{b}$, and specified the relationship $\underline{b} = \underline{\underline{A}}\,\underline{x}$. This section describes how we estimate the change image $\underline{x}$ from measurements $\underline{b}$.

The change image, $\underline{x}$, is by its definition sparse, having only a few pixels with non-zero energy that explain the data. We exploit this sparseness in a basis pursuit denoising framework to estimate $\underline{x}$, i.e., we estimate $\underline{x}$ by solving

$$\text{argmin}_{\underline{x}} \left\|\underline{x}\right\|_1 \qquad s.t. \qquad \left\|\underline{\underline{A}}\underline{x} - \underline{b}\right\|_2 \leq \sigma. \quad (12)$$

We use the toolset described in [7] and implemented in a code base called *SPGL1*. This toolset achieves the solution by solving a sequence of LASSO problems

$$\min_{\underline{x}} \left\|\underline{\underline{A}}\underline{x} - \underline{b}\right\|_2 \qquad s.t. \qquad \left\|\underline{x}\right\|_1 \leq \tau, \quad (13)$$

via a spectral projected-gradient algorithm. Each of the solutions generates an update to a Newton root-finding algorithm that converges on the location where the residual $\left\|\underline{\underline{A}}\underline{x} - \underline{b}\right\|_2$ is below the noise tolerance σ.

D. Comparison to Backprojection Imaging

Backprojection imaging [8] is a standard approach which provides a useful comparison to our proposed sparse-model method. Backprojection applies an inverse model that maps from measurements $\underline{b}$ to the unknowns $\underline{x}$,

$$\underline{x} = \underline{\underline{S}}\,\underline{b}, \quad (14)$$

to estimate the unknowns $\underline{x}$, where $\underline{\underline{S}}$ is another selection matrix. Here $\underline{\underline{S}}$ selects which measurements i correspond to ground pixels j. This is the opposite of our forward-model approach (eq. (9)), which employs a selection matrix defining how ground pixels correspond to measurements.

Backprojection corresponds to an L_2 minimization on $\underline{x}$ rather than an L_1 minimization, i.e., it solves an equation of the form

$$\text{argmin}_{\underline{x}} \left\|\underline{x}\right\|_2 \qquad s.t. \qquad \left\|\underline{\underline{Q}}\underline{x} - \underline{b}\right\|_2 \leq \sigma. \quad (15)$$

III. Experimental Results

The experiments we describe here employ a commercially available *AKELA AVMU500A* radar along with *4 SAS-510-4* antennas. The antennas are directional and are specified to have a *3dB* point of *41* degrees by the manufacturer. The system was selected because its size and versatility demonstrate the ability of a compact, contained system to effectively collect the necessary data.

The radar is a stepped CW type, capable of transmitting pulses between *300MHz* and *3GHz*. The rate at which the individual frequencies are sampled is selectable, set here at *45kHz*. The radar has four ports, any of which may be used for transmit or receive; however, because the radar has only one transmitter and receiver, it is not possible to receive multiple ports simultaneously. Therefore the collections will transmit and receive between one pair, and then move to transmit and receive to the next pair, and so on. Since this happens at a very fast rate compared to the dismount speed, the measurements are well approximated as being simultaneous. Figure 2 shows the AKELA unit.

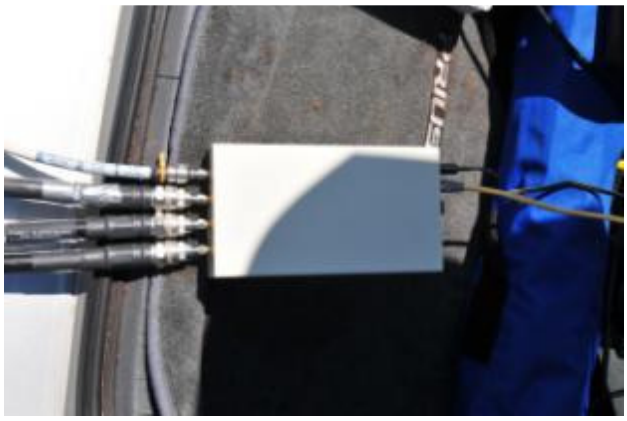

Figure 2. AKELA AVMU500A Radar Unit.

A. High-RCS Cylinder Change Detection

This first experiment shows change imager computed for a large RCS target. Four antennas were arranged around the perimeter of a surveillance region as illustrated in Figure 3. The antennas extended approximately $30m$ in the north-to-south direction and $10m$ is the east-to-west direction. Their position was recorded with a handheld GPS and differentially corrected. The imaging region was offset about $20m$ in the east-west direction and about $30mx30m$ in size. An image of the scene as viewed from Antenna 3 is show in Figure 4.

Two collections of the scene were taken. The first collection was a reference (empty) scene and the second (change) scene had a large cylinder at scene center, as shown in Figure 4. The true position of the cylinder was recorded using a handheld GPS, and differentially corrected. Each collection used $2GHz$ of bandwidth around a $2GHz$ center frequency with 1670 narrowband step frequencies. Data was collected from the 6 unique bistatic pairs (no monostatic data was collected).

Figure 3. The layout of the four antennas.


Figure 4. The surveillance region, viewed from the perspective of Antenna 3 after a large cylinder (the change) was added to the scene.

The measurement vector $\underline{b}$ was formed by first creating the calibrated range profile for each transmit-receive pair for both the reference and change collections. This is accomplished by Fourier transforming the raw frequency response data, averaging over 100 pulses and rescaling using the appropriate transmit/receive pair calibration scalar. Next, the difference data was created by coherently subtracting the reference data from the change data. Since data from the radar starts at range 0 and goes to the unambiguous range, the data was further reduced by removing range bins outside the imaging scene. Finally, the data was ordered to conform to the convention defined earlier, resulting in the $\underline{b}$ vector of difference measurements shown in Figure 5.

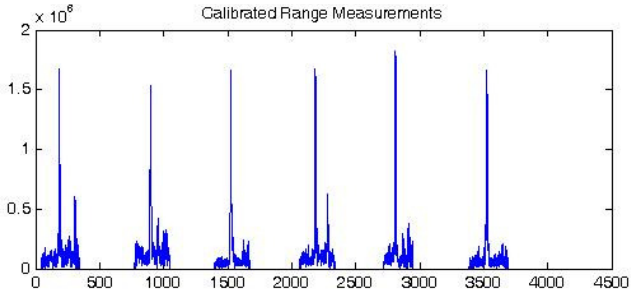

Figure 5. Calibrated, range profile difference measuremnet vector $\underline{b}$.

Figure 6 shows a portion of the $\underline{\underline{A}}$ matrix for transmit-receive antenna pair 1→4 over the scene. The selection matrix is very sparse. It is only non-zero at locations where the transmitter/receiver/range bin specified by i corresponds to the x, y location specified by j. In practice, the matrix does not ever have to be actually formed in memory, only methods which compute the product between the matrix and an arbitrary vector $\underline{x}$.


Figure 6. Part of the selection matrix $\underline{\underline{A}}$ for an Isotropic Scattering Model. Rows correspond to measurements and columns to spatial locations.

The *SPGL1* codeset was used to find the unknown vector $\underline{x}$. As discussed earlier, the solver uses an iterative approach with a convergence criterion to determine when a solution has been found. This convergence criterion is based on the residual error between the truth measurement vector $\underline{b}$ and the *SPGL1* measurement vector calculated by multiplying the transfer function $\underline{\underline{A}}$ by the $\underline{x}$ vector of unknowns. Figure 7 shows the truth and measurement vectors along with the difference between the two. Note that the measurements are on the order of 10^5 whereas the differences are on the order 10^1.

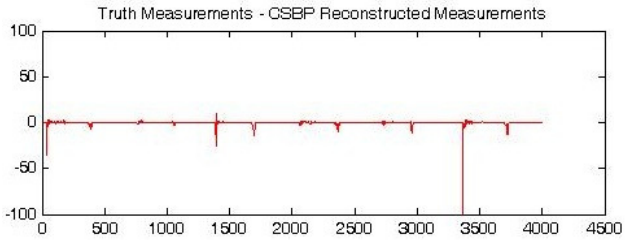

Figure 7. Truth Measurements vs Reconstructed Measurements.

The final sparse $\underline{x}$ vector of unknowns is reshaped into a change image. It represents the sparsest set of isotropic scatters required to represent the difference measurements.

Figure 8 shows backprojection and sparse-model change images created from this data collection. A change was introduced at (0,0). The backprojection change image is formed using the toolbox described in [8], modified to allow bistatic measurements. It shows a recognizable change at (0,0), but also includes strong lines of constant bistatic range because of the very poor sampling in aperture. In contrast, the sparsity-constrained change image shows excellent location of the change without these artifacts.

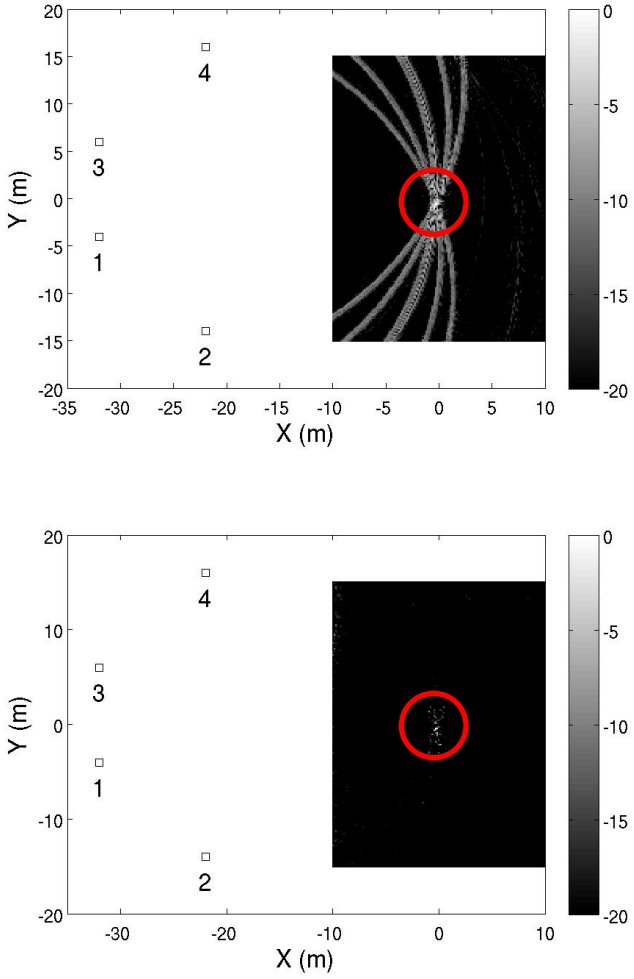

Figure 8. Backprojection (Top) and sparsity-constrained (Bottom) change images corresponding to a cylinder placed at (0,0). The images are scaled 20dB down from their max. The cylinder location is circled for reference. The sparsity-constrained image significantly improves the change image.

B. *Dismount Change Detection*

This second experiment shows change imagery for a scene that has a person in it. Four antennas were arranged around the perimeter of the surveillance region in the configuration illustrated in Figure 9.

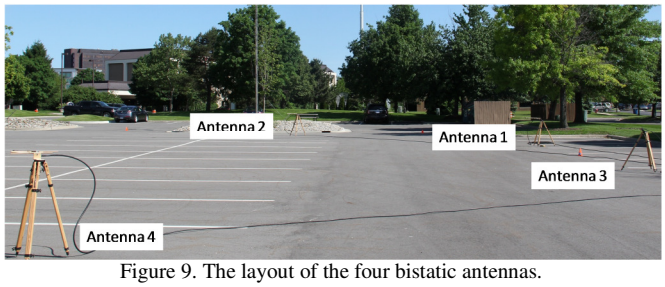

Figure 9. The layout of the four bistatic antennas.

Two collections of the scene were taken. The first collection was a reference (empty) scene and the second (change) scene had a person at scene center, as shown in Figure 11. An interesting property of this springtime collect is that a persistent change is present in the imagery – a fully foliated tree that blows in the wind causing changes in bistatic range measurements in its vicinity. Figure 10 shows two images of the tree taken a few seconds apart, illustrating how the leaves moved.

Figure 10. Spatially aligned images of the tree, taken a few seconds apart show that the leaves have moved significantly.

The true position of the antennas, person, and the tree were recorded using both hand and GPS measurements. Data was collected with *1GHz* of bandwidth around a *1.5GHz* center frequency with *800* step frequencies from the *6* unique bistatic pairs. Figure 12 shows the change image computed using conventional back-projection imaging and our sparsity-constrained method. While the change regions are identifiable in the backprojection image, the overall utility of the image is very poor because of the lines of constant bistatic range. The sparsity constrained image, however is able to accurately identify just the change regions.

Figure 11. Image after the change. The location of the dismount and the tree are circled.

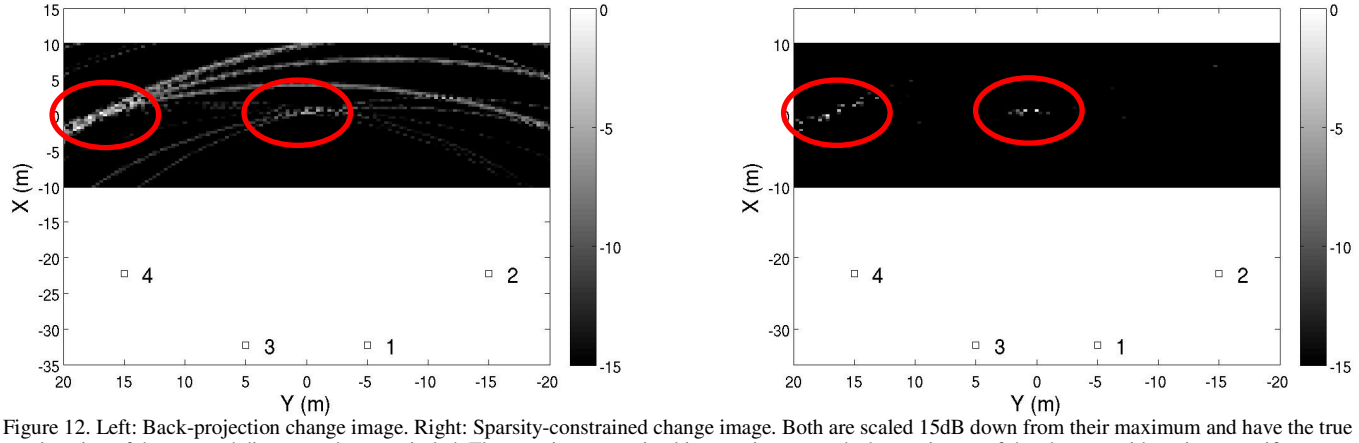

Figure 12. Left: Back-projection change image. Right: Sparsity-constrained change image. Both are scaled 15dB down from their maximum and have the true location of the tree and dismount changes circled. The sparsity-constrained image gives a much sharper image of the changes without image artifacts.

IV. Conclusions

This paper describes a sparse imaging approach for estimating change images from a constellation of multistatic radar. In our setup, radar antennas are arranged around the perimeter of a surveillance region. This provides large angular diversity but a very small angular sampling over the large aperture. Conventional backprojection imaging techniques applied to this data produce very large sidelobes and other image artifacts, severely degrading the utility of the imagery. We describe an innovative imaging method which formulates the problem of estimating the change image from one collection to another as a sparsity-constrained estimation problem. We illustrate the method with collected data, and show that the sparseness constraint produces excellent images with very limited sampling of the aperture.

Acknowledgment

The authors would like to thank Dr. Benjamin Shapo for helpful discussions regarding this work.

References

[1] W. Carrera, R. Goodman, and R. Majewski, "Spotlight synthetic aperture radar: signal processing algorithms". Artech House, 1995.

[2] W. Rao, G. Li, X. Wang, X. Xia, and G. Xiang, "ISAR imaging of maneuvering targets with missing data via matching pursuit", *2011 IEEE Radar Conference*, pp. 124-128.

[3] P. Khomchuk, I. Bilik, I.; and D. P. Kasilingan., "Compressive Sensing-based SAR Tomography", *2010 IEEE Radar Conference*, pp. 124-128, pp. 354-358.

[4] H. A. Krichene, et. al., "Compressive sensing and stretch processing", *2011 IEEE Radar Conference*, pp. 362-367.

[5] L. Wang, and B. Yazici, "Bistatic Synthetic Aperture Radar imaging using ultranarrow-band continuous waveforms", 2011 *IEEE Radar* Conference, pp. 62-67.

[6] L. Wang, M. Cheney, and B. Borden, "Multistatic radar imaging of moving targets", 2010 IEEE Radar Conference, pp. 391-396.

[7] E. van den Berg, M.P. Friedlander, "Probing the Pareto frontier for basis pursuit solutions", SIAM Journal on Scientific Computing, 31(2), 2008, 890—912.

[8] L. Gorham and L. Moore, "SAR image formation toolbox for MATLAB", Proceedings of SPIE, April 2010.

[9] M. I. Skolnik, Radar Handbook, Second Edition, Boston: McGraw Hill, 1990, Chapter 25.

[10] B. Shapo and C. Kreucher, "Basis Pursuit for Robust Passive Acoustic Beamforming". Proceedings of the 43rd Asilomar Conference on Signals, Systems and Computers, pp. 472-476, November 1-4 2009.

[11] N. Willis and H. Griffiths, Advances in Bistatic Radar, SciTech Pub. Inc., 2007.

[12] A. Gurbuz, J. McClellan, and W. Scott, "A Compressive Sensing Data Acquisition and Imaging Method for Stepped Frequency GPRs", IEEE Trans. Signal Processing, vol. 57, no. 7, July 2009.